bond with the main chain of Lys39. In summary, 8-oxo-dGMP is surrounded by 12 types of hydrogen bonds. The hydrogen-bonding interactions with the pyrimidine moiety and the α-phosphate group in MutT-8-oxo-dGMP are similar to those with the corresponding pyrimidine moieties and α-phosphate groups in the structures of BdRppH-GTP-Mg^{2+} and BdRppH-dGTP (BdRppH-(d)GTPs) (40). The positions of the base moieties of (d)GTPs with the *syn* conformation in BdRppH-(d)GTPs accord with that of 8-oxo-dGMP in MutT-8-oxo-dGMP with a rmsd of 0.6 Å for the corresponding 11 atoms when proteins are superimposed. BdRppH with Arg40, Phe52, and Asn136 residues corresponding to Arg23, Phe35, and Asn119 of MutT, respectively, recognizes N1-H, N2-H, and O6 of the pyrimidine moiety by four hydrogen bonds with Phe52 and Asn136; Pα-O of the α-phosphate group is recognized by a hydrogen bond with Arg40. This recognition mode is the same as that observed in MutT. Apart from the similarities, differences are found in recognition of the imidazole moiety of the base and the sugar moiety as well as in the ligand-induced conformational change. The imidazole and sugar moieties of (d)GTPs in BdRppH-(d)GTPs do not form hydrogen bonds with any residues in BdRppH. In addition, although ligand-induced conformational change with loop ordering is observed in BdRppH, the change is significantly small (ca. 2~4 Å) as compared to that in MutT. The large ligand-induced conformational change observed in MutT does contribute to its high affinity for 8-oxoG nucleotides, as discussed below. There is a large discrepancy between the K_m values of 0.081 and 268 μM for the hydrolysis of 8-oxo-dGTP by MutT and of dGTP by BdRppH, respectively (7,44). This may derive from these structural differences, in addition to the unfavorable *syn* conformation of (d)GTPs in BdRppH-(d)GTPs.

As a result of the strict recognition of 8-oxo-dGMP with the large conformational change, there are low B factors and unambiguous electron densities around 8-oxo-dGMP (supplemental Fig. S1B, Fig. 3E). The average B factor of 8-oxo-dGMP is 12.4 $Å^2$ and that of the residues involved in the recognition of 8-oxo-dGMP, Arg23, His28, Phe35, Asp77, Arg78, and Asn119 is 13.6 $Å^2$. These low B factors and unambiguous electron densities represent the small thermal motion and/or the ordered positioning of 8-oxo-dGMP and the residues of the active site in the crystal lattice. This phenomenon explains isothermal titration calorimetry (ITC) experiments (45), indicating that the tight binding of 8-oxo-dGMP to MutT ($\Delta\Delta G$ = –9.8 kcal/mol) is driven by a highly favorable enthalpy (ΔH = –39.0 kcal/mol) with an unfavorable entropy ($-T\Delta S$ = 29.2 kcal/mol). The unfavorable entropy would be a result of the conformational rigidity generated from the connection of loops L-A and L-D with large ligand-induced conformational changes. On the other hand, the more favorable enthalpy would be produced by the large number of hydrogen bonds and van der Waals interactions formed between 8-oxo-dGMP and MutT; this is sufficient to compensate for the unfavorable entropy and to bind tightly.

Furthermore, the hydrogen bond-mediated recognition mode found in MutT-8oxo-dGMP is comparable with the results of mutational studies in which it was found that the R78A, N119D, and N119A mutants show 7-, 37-, and 1650-fold decreases in affinity for 8-oxo-dGMP in comparison with the wild-type and that they lose binding free energies ($\Delta\Delta G$) of 1.1, 2.1, and 4.3 kcal/mol, respectively, as measured by the increases in K_I (46). According to previous reports, the contribution of the hydrogen bond to protein stability can be estimated as ca. 2 and 1.2 kcal/mol for hydrogen bonds between protein residues and for those between a water molecule and a protein residue, respectively (47,48). Judging from the MutT-8oxo-dGMP structure, the N119D and N119A mutants lose one hydrogen bond between the O6 of 8-oxo-dGMP and the Nδ-H of Asn119 and two hydrogen bonds involving the O6 and N7-H of 8-oxo-dGMP and the amide group of Asn119, respectively (Fig. 3C). The R78A mutant loses the hydrogen bond to a water molecule (Fig. 3C); that is, $\Delta\Delta G$ losses of 1.2, 2, and 4 kcal/mol are estimated for the R78A, N119D, and N119A mutants, respectively; this agrees perfectly with the experimental data (46).

The feature of the substrate-binding site in

MutT-8-oxo-dGMP is also consistent with reports that MutT hydrolyzes both deoxyribose and ribose derivatives of 8-oxoG nucleotides with similar efficiency (2,7). This is because in spite of a number of hydrogen-bonding interactions between 8-oxo-dGMP and MutT, there is space for a hydroxyl group instead of the hydrogen atom at the 2′ position of the sugar ring (Fig. 3B).

This recognition mechanism of 8-oxo-dGMP by MutT is different from any models predicted by NMR studies (PDB ID 1PPX, 1PUN, 1PUQ, 1PUS, and 1MUT) (supplemental Fig. S3).

Discrimination of 8-oxoG nucleotides from G nucleotides— The K_m values of *E. coli* MutT for 8-oxo-dGTP and 8-oxo-GTP are ca. 3,800- to 14,000-fold lower than the values for the corresponding G nucleotides (7). These data agree with the observation that the K_d value (52 nM) between 8-oxo-dGMP and MutT is 34,000-fold lower than that (1.76 mM) between dGMP and MutT (45). Thus, the most important question that this study addresses is the mechanism by which MutT obtains high substrate specificity for 8-oxoG nucleotides as compared with G nucleotides.

According to the recognition scheme of 8-oxo-dGMP by MutT, the major difference in the recognition of 8-oxoG versus G is whether the single hydrogen bond between Oδ of Asn119 and N7-H of 8-oxoG occurs or not. This situation is similar to those of OGG1, MutM, and MutY (13,15,16). If the side chain conformation of Asn119 in the MutT complex with G nucleotides was the same as that in the MutT-8-oxo-dGMP structure, the two lone pairs at N7 of G and Oδ of Asn119 would be repulsive (supplemental Fig. S4). In order to avoid this repulsion, a rotation about the side chain torsion angles in Asn119 should be required. Thus, the difference in the number of hydrogen bonds formed between MutT–G and MutT–8-oxoG complexes is only one. The contribution of one hydrogen bond to ΔΔG is estimated to be 2 kcal/mol (47,48).

The *syn* glycosidic conformation of 8-oxo-dGMP must also be one of the elements contributing to the substrate specificity of MutT because 8-oxoG nucleotides favor a *syn* conformation by the steric hindrance between O8 and the sugar moiety; this is in contrast with G nucleotides that adopt both *syn* and *anti* conformations (49,50). Because of the lack of quantitative data on the preference of the *syn* conformation about the 8-oxoG nucleotides, it is difficult to estimate the free energy difference between the *syn* and *anti* conformations. However, it is unlikely that the preference of MutT for the *syn* conformation over the *anti* conformation is more than 10-fold ($\Delta\Delta G \approx 1.4$ kcal/mol) because the *anti* conformation for 8-oxoG nucleotides is sometimes observed in the crystal structures of 8-oxoG recognition complexes such as OGG1 and MutY (15,16).

These discrimination factors cannot by themselves explain the roughly 34,000-fold difference between the binding affinity of MutT for 8-oxo-dGMP and dGMP ($\Delta\Delta G \approx 6$ kcal/mol). When 8-oxo-dGMP binds to MutT, large ligand-induced conformational changes with an ordering of loop regions are observed. On the other hand, in the binding of dGMP to MutT, the thermal parameters of $\Delta G = -3.7$, $\Delta H = -3.3$, and $-T\Delta S = -0.4$ kcal/mol; the changes in backbone ^{15}N and NH chemical shifts in 22 residues; and the slowing down of the NH exchange with D_2O of 20 residues are remarkably different when compared with the changes (the thermal parameters of $\Delta G = -9.8$, $\Delta H = -39.0$, and $-T\Delta S = 29.2$ kcal/mol; the changes in backbone ^{15}N and NH chemical shifts in 62 residues; and the slowing down of the NH exchange with D_2O of 45 residues) involved in the binding of 8-oxo-dGMP to MutT (19,45). These facts suggest that no significant conformational change in MutT is observed when dGMP binds to MutT. The large ligand-induced conformational change in MutT also contributes to the discrimination of 8-oxoG nucleotides from G nucleotides.

A comparison of the amino acid sequences of MutT-related enzymes suggests that the enzymes with higher substrate specificity for 8-oxoG are only MutT homologs from closely related species with conserved amino acids in the positions that participate in the recognition of 8-oxoG and the conformational change (Fig. 1, green asterisk). In fact, these amino acids are not highly conserved among *E. coli* Orf135 (51),

Bacillus subtilis YtkD (52), and hMTH1 (8) that have broad substrate specificities.

Structure of the MutT signature and metal-binding sites— We have solved two types of Mn^{2+}-bound structures, MutT-8-oxo-dGMP-Mn^{2+} and MutT-Mn^{2+}, in order to determine metal-binding sites at the MutT signature of MutT. The crystal of MutT-Mn^{2+} contains two proteins per asymmetric unit. Their overall structures are very similar, with the rmsd of 0.3 Å for the corresponding 118 Cα atoms; for simplicity, only one molecule will be referred to in all further discussion. The structure of MutT-Mn^{2+} is similar to that of the apo form, with rmsd of 0.6 Å for the corresponding 118 Cα atoms.

In the MutT signature having an SLHL structure (Fig. 4A), Gly38, Glu44, Arg52, Glu53, Glu56, Glu57, and Gly59 are completely conserved among the members of the Nudix family (Fig. 1). The SLHL structure of MutT is similar to those of other enzymes in the Nudix family. For example, the conserved 23 residues can be superimposed on ones found in the *Pyrobaculum aerophilum* nudix protein with an rmsd of 0.5 Å (53). A characteristic feature in the SLHL structure is the hydrogen-bonding network centering on the converged Arg52 that anchors α-1 to its connecting loop. The side chains of Glu44 and Arg52, which form two hydrogen bonds with each other, participate in hydrogen bonding to the main chain atoms in the nonconserved Glu41 and Lys39 residues, respectively. Arg52 also interacts with the side chains of the conserved Glu53 and Glu56 residues (Fig. 4A). This hydrogen bonding network is roughly the same as that in the other Nudix proteins and contributes to the conformational stability of the SLHL structure (39,40,53-65).

In the electron density maps of the MutT-Mn^{2+} crystal produced by co-crystallization, there were three peaks corresponding to the metal ions near the MutT signature. Judging from the peak heights, B factors, bond lengths, and bond angles, we determined that two peaks were Mn^{2+} ions (nearly ideal octahedral coordination and an average bond length of approximately 2.2 Å) and one was Na^{+} (distorted octahedral coordination and an average bond length of approximately 2.5 Å) (Fig. 4B). Furthermore, the two Mn^{2+} sites were also confirmed from significant densities (more than 10 σ level) on the anomalous difference Fourier map at λ = 1 Å (data not shown). On the other hand, the densities of the Na^{+} site were less than noise level. The refined MutT-Mn^{2+} structure reveals that two Mn^{2+} ions form a binuclear metal center with a bridged water molecule. One Mn^{2+} coordinates to the oxygen atoms of Glu53, Glu57, three water molecules, and Asp77 in another molecule (Asp77*). The coordination partners of another Mn^{2+} are Glu53, L-tartrate (a crystallization reagent), and four water molecules. Na^{+} coordinates to the oxygen atoms of Gly37, Glu57, Asp77*, and two water molecules. Asp77* and L-tartrate bind to the MutT signature through metal ions, but do not distort the SLHL structure.

In the MutT-8-oxo-dGMP-Mn^{2+} crystal (prepared by soaking MutT-8-oxo-dGMP crystals in reservoir supplemented with 1 mM $MnCl_2$), Mn^{2+} binds to the six oxygen atoms of the main chain of Gly37, the side chain of Glu57, the phosphate group, and three water molecules with nearly ideal octahedral coordination (Fig. 4A). The binding of Mn^{2+} to the MutT-8-oxo-dGMP binary complex makes the phosphate group move slightly toward Mn^{2+} (the P atom moves by 0.7 Å). The position of Mn^{2+} observed in MutT-8-oxo-dGMP-Mn^{2+} is close to that of Na^{+} in MutT-Mn^{2+} (at a distance of 1.4 Å). The three Mn^{2+} binding sites consisting of the Mn^{2+} in MutT-8-oxo-dGMP-Mn^{2+} and two additional Mn^{2+} ions in MutT-Mn^{2+} (Fig. 4C) are located at common metal-binding sites observed in the Nudix family (60) and correspond to those observed in the ternary complexes of *E. coli* ADP-ribose pyrophosphatase (ADPRase), *Mycobacterium tuberculosis* ADPRase, *Caenorhabditis elegans* Ap_4A hydrolase, *Xenopus laevis* X29, human NUDT5, *Thermus thermophilus* Ndx2, and BdRppH (40,55,57,64-67). Thus, the three sites are considered to be candidates for metal-binding in 8-oxo-dGTP hydrolysis. Previous kinetic studies have shown that MutT binds to one Mn^{2+} in the absence of nucleotides and two Mn^{2+} ions in the presence of a nonspecific substrate analog,

AMPCPP (68). The middle Mn^{2+} (Mn2 in Fig. 4C) may be prebound to the active site, judging from the number of coordination partners in MutT and the Mn^{2+} ion (Mn1 in Fig. 4C) found in MutT-8-oxo-dGMP-Mn^{2+}; otherwise, it and other Mn^{2+} ion (Mn1 and Mn3, respectively in Fig. 4C) would be recruited with the substrate. The probability of the three metals binding to MutT in the presence of the real substrate 8-oxo-dGTP can not be neglected because of the fact that the number of binding metals depends on the kinds of substrate analogs (40,54,60,61,64-66).

The structures of MutT-8-oxo-dGMP-Mn^{2+} and MutT-Mn^{2+} suggest structural insights into some essential or important residues for the 8-oxo-dGTP hydrolysis. Glu53 and Glu57 are essential for the suppression of spontaneous A:T to C:G transversion mutations (69), and E53Q and E57Q mutants decrease k_{cat} by 10^4 ~ 10^5-fold (70). On the other hand, Glu56 is nonessential for the suppression of the mutations (69), and E56Q and E98Q mutants have relatively small effects (< 24-fold) on k_{cat} (70). These results agree with our structural studies showing that essential residues, Glu53 and Glu57, directly bind to metal ions whereas important residues, Glu56 and Glu98, make water-mediated interactions with metal ions (Fig. 4A, B). Gly37 and Gly38, which are located at the surface of the ligand-binding site, are also revealed to be essential residues for the suppression of the mutations (69). The side chains of any residues except Gly in positions 37 and 38 would contact the base moiety of the nucleotide ligand and the essential residue for the catalysis, Glu53, respectively (Fig. 4A, C). For this reason, in order to express 8-oxo-dGTPase activity, residues 37 and 38 must be Gly, which has the smallest side chain.

A number of kinetic, mutational, and NMR studies of MutT using dGTP and/or a substrate analog, AMPCPP, have been reported, and a catalytic mechanism is proposed by Mildvan and coworkers (71). Compared to our structural data, there appear to be some differences in the metal-binding sites. Gly38 is involved in metal coordination in their model, but Gly37, instead of Gly38, is a metal ligand in the structure of MutT-8-oxo-dGMP-Mn^{2+} (Fig. 4A, C). The all-crystal structures of Nudix proteins show that the carbonyl oxygen of the corresponding residue to Gly38 participates in the formation of β-sheet whereas that of Gly37 binds to a metal ion (40,55,57-59,61,64-67). Glu56 and Glu98, which are metal ligands in the model proposed by Mildvan and coworkers, interact with water molecules bound to metal ions in our structures. The metal coordination scheme changes in the active site during the reaction, and a more proper enzymatic mechanism activated by metal ions might be examined by kinetic protein crystallography.

REFERENCES

1. Maki, H., and Sekiguchi, M. (1992) *Nature* 355(6357), 273-275
2. Taddei, F., Hayakawa, H., Bouton, M., Cirinesi, A., Matic, I., Sekiguchi, M., and Radman, M. (1997) *Science* 278(5335), 128-130
3. Au, K. G., Cabrera, M., Miller, J. H., and Modrich, P. (1988) *Proc. Natl. Acad. Sci. U. S. A.* 85(23), 9163-9166
4. Cabrera, M., Nghiem, Y., and Miller, J. H. (1988) *J. Bacteriol.* 170(11), 5405-5407
5. Michaels, M. L., Cruz, C., Grollman, A. P., and Miller, J. H. (1992) *Proc. Natl. Acad. Sci. U. S. A.* 89(15), 7022-7025
6. Tchou, J., Kasai, H., Shibutani, S., Chung, M. H., Laval, J., Grollman, A. P., and Nishimura, S. (1991) *Proc. Natl. Acad. Sci. U. S. A.* 88(11), 4690-4694

7. Ito, R., Hayakawa, H., Sekiguchi, M., and Ishibashi, T. (2005) *Biochemistry* 44(17), 6670-6674
8. Fujikawa, K., Kamiya, H., Yakushiji, H., Fujii, Y., Nakabeppu, Y., and Kasai, H. (1999) *J. Biol. Chem.* 274(26), 18201-18205
9. Fujikawa, K., Kamiya, H., Yakushiji, H., Nakabeppu, Y., and Kasai, H. (2001) *Nucleic Acids Res.* 29(2), 449-454
10. Mishima, M., Sakai, Y., Itoh, N., Kamiya, H., Furuichi, M., Takahashi, M., Yamagata, Y., Iwai, S., Nakabeppu, Y., and Shirakawa, M. (2004) *J. Biol. Chem.* 279(32), 33806-33815
11. Tchou, J., Bodepudi, V., Shibutani, S., Antoshechkin, I., Miller, J., Grollman, A. P., and Johnson, F. (1994) *J. Biol. Chem.* 269(21), 15318-15324
12. Hatahet, Z., Kow, Y. W., Purmal, A. A., Cunningham, R. P., and Wallace, S. S. (1994) *J. Biol. Chem.* 269(29), 18814-18820
13. Fromme, J. C., and Verdine, G. L. (2003) *J. Biol. Chem.* 278(51), 51543-51548
14. Porello, S. L., Leyes, A. E., and David, S. S. (1998) *Biochemistry* 37(42), 14756-14764
15. Bruner, S. D., Norman, D. P., and Verdine, G. L. (2000) *Nature* 403(6772), 859-866
16. Fromme, J. C., Banerjee, A., Huang, S. J., and Verdine, G. L. (2004) *Nature* 427(6975), 652-656
17. Bessman, M. J., Frick, D. N., and O'Handley, S. F. (1996) *J. Biol. Chem.* 271(41), 25059-25062
18. Abeygunawardana, C., Weber, D. J., Gittis, A. G., Frick, D. N., Lin, J., Miller, A. F., Bessman, M. J., and Mildvan, A. S. (1995) *Biochemistry* 34(46), 14997-15005
19. Massiah, M. A., Saraswat, V., Azurmendi, H. F., and Mildvan, A. S. (2003) *Biochemistry* 42(34), 10140-10154
20. Doublie, S. (1997) *Methods Enzymol.* 276, 523-530
21. LeMaster, D. M., and Richards, F. M. (1985) *Biochemistry* 24(25), 7263-7268
22. Nakamura, T., Kitaguchi, Y., Miyazawa, M., Kamiya, H., Toma, S., Ikemizu, S., Shirakawa, M., Nakabeppu, Y., and Yamagata, Y. (2006) *Acta Crystallogr.* F62, 1283-1285
23. Akiyama, M., Maki, H., Sekiguchi, M., and Horiuchi, T. (1989) *Proc. Natl. Acad. Sci. U. S. A.* 86(11), 3949-3952
24. Nakamura, T., Doi, T., Sekiguchi, M., and Yamagata, Y. (2004) *Acta Crystallogr.* D60, 1641-1643
25. Rossmann, M. G., and van Beek, C. G. (1999) *Acta Crystallogr.* D55, 1631-1640

26. Otwinowski, Z., and Minor, W. (1997) *Methods Enzymol.* 276, 307-326
27. Matthews, B. W. (1968) *J. Mol. Biol.* 33(2), 491-497
28. Terwilliger, T. C., and Berendzen, J. (1999) *Acta Crystallogr.* D55, 849-861
29. Collaborative Computational Project, Number 4. (1994) *Acta Crystallogr.* D50, 760-763
30. Cowtan, K. (1994) *Joint CCP4 and ESF-EACBM Newsletter on Protein Crystallography* 31, 34-38
31. Cambillau, C., Horjales, E., and Jones, T. A. (1984) *Journal of Molecular Graphics* 2(2), 53-54
32. Jones, T. A., Zou, J. Y., Cowan, S. W., and Kjeldgaard, M. (1991) *Acta Crystallogr A* 47 (Pt 2), 110-119
33. Brunger, A. T. (1992) *Yale Univ. Press, New Haven, CT*
34. Brunger, A. T., Adams, P. D., Clore, G. M., DeLano, W. L., Gros, P., Grosse-Kunstleve, R. W., Jiang, J. S., Kuszewski, J., Nilges, M., Pannu, N. S., Read, R. J., Rice, L. M., Simonson, T., and Warren, G. L. (1998) *Acta Crystallogr.* D54, 905-921
35. Navaza, J. (1994) *Acta Crystallogr.* A50, 157-163
36. Laskowski, R. A., MacArthur, M. W., Moss, D. S., and Thornton, J. M. (1993) *J. Appl. Crystallogr.* 26, 283-291
37. Kabsch, W. (1976) *Acta Crystallogr A* 32, 922-923
38. DeLano, W. L. *The PyMOL Molecular Graphics System*, http://pymol.sourceforge.net/
39. Gabelli, S. B., Bianchet, M. A., Xu, W., Dunn, C. A., Niu, Z. D., Amzel, L. M., and Bessman, M. J. (2007) *Structure* 15(8), 1014-1022
40. Messing, S. A., Gabelli, S. B., Liu, Q., Celesnik, H., Belasco, J. G., Pineiro, S. A., and Amzel, L. M. (2009) *Structure* 17(3), 472-481
41. Holm, L., Kaariainen, S., Rosenstrom, P., and Schenkel, A. (2008) *Bioinformatics* 24(23), 2780-2781
42. Bhatnagar, S. K., Bullions, L. C., and Bessman, M. J. (1991) *J Biol Chem* 266(14), 9050-9054
43. Saenger, W. (1984) *Principles of Nucleic Acid Structure*
44. Steyert, S. R., Messing, S. A., Amzel, L. M., Gabelli, S. B., and Pineiro, S. A. (2008) *J Bacteriol* 190(24), 8215-8219
45. Saraswat, V., Massiah, M. A., Lopez, G., Amzel, L. M., and Mildvan, A. S. (2002) *Biochemistry* 41(52), 15566-15577

46. Saraswat, V., Azurmendi, H. F., and Mildvan, A. S. (2004) *Biochemistry* 43(12), 3404-3414
47. Funahashi, J., Takano, K., Yamagata, Y., and Yutani, K. (2002) *J. Biol. Chem.* 277(24), 21792-21800
48. Takano, K., Yamagata, Y., Funahashi, J., Hioki, Y., Kuramitsu, S., and Yutani, K. (1999) *Biochemistry* 38(39), 12698-12708
49. Kouchakdjian, M., Bodepudi, V., Shibutani, S., Eisenberg, M., Johnson, F., Grollman, A. P., and Patel, D. J. (1991) *Biochemistry* 30(5), 1403-1412
50. Uesugi, S., Yano, J., Yano, E., and Ikehara, M. (1977) *J. Am. Chem. Soc.* 99(7), 2313-2323
51. Kamiya, H., Murata-Kamiya, N., Iida, E., and Harashima, H. (2001) *Biochem Biophys Res Commun* 288(3), 499-502
52. Xu, W., Jones, C. R., Dunn, C. A., and Bessman, M. J. (2004) *J Bacteriol* 186(24), 8380-8384
53. Wang, S., Mura, C., Sawaya, M. R., Cascio, D., and Eisenberg, D. (2002) *Acta Crystallogr.* D58, 571-578
54. Gabelli, S. B., Bianchet, M. A., Bessman, M. J., and Amzel, L. M. (2001) *Nat. Struct. Biol.* 8(5), 467-472
55. Bailey, S., Sedelnikova, S. E., Blackburn, G. M., Abdelghany, H. M., Baker, P. J., McLennan, A. G., and Rafferty, J. B. (2002) *Structure (Camb.)* 10(4), 589-600
56. Kang, L. W., Gabelli, S. B., Bianchet, M. A., Xu, W. L., Bessman, M. J., and Amzel, L. M. (2003) *J. Bacteriol.* 185(14), 4110-4118
57. Kang, L. W., Gabelli, S. B., Cunningham, J. E., O'Handley, S. F., and Amzel, L. M. (2003) *Structure (Camb.)* 11(8), 1015-1023
58. Shen, B. W., Perraud, A. L., Scharenberg, A., and Stoddard, B. L. (2003) *J. Mol. Biol.* 332(2), 385-398
59. Gabelli, S. B., Bianchet, M. A., Azurmendi, H. F., Xia, Z., Sarawat, V., Mildvan, A. S., and Amzel, L. M. (2004) *Structure (Camb)* 12(6), 927-935
60. Ranatunga, W., Hill, E. E., Mooster, J. L., Holbrook, E. L., Schulze-Gahmen, U., Xu, W., Bessman, M. J., Brenner, S. E., and Holbrook, S. R. (2004) *J. Mol. Biol.* 339(1), 103-116
61. Yoshiba, S., Ooga, T., Nakagawa, N., Shibata, T., Inoue, Y., Yokoyama, S., Kuramitsu, S., and Masui, R. (2004) *J. Biol. Chem.* 279(35), 37163-37174
62. She, M., Decker, C. J., Chen, N., Tumati, S., Parker, R., and Song, H. (2006) *Nat. Struct. Mol. Biol.* 13(1), 63-70

63. Zha, M., Zhong, C., Peng, Y., Hu, H., and Ding, J. (2006) *J Mol Biol* 364(5), 1021-1033
64. Scarsdale, J. N., Peculis, B. A., and Wright, H. T. (2006) *Structure* 14(2), 331-343
65. Wakamatsu, T., Nakagawa, N., Kuramitsu, S., and Masui, R. (2008) *J Bacteriol* 190(3), 1108-1117
66. Gabelli, S. B., Bianchet, M. A., Ohnishi, Y., Ichikawa, Y., Bessman, M. J., and Amzel, L. M. (2002) *Biochemistry* 41(30), 9279-9285
67. Zha, M., Guo, Q., Zhang, Y., Yu, B., Ou, Y., Zhong, C., and Ding, J. (2008) *J Mol Biol* 379(3), 568-578
68. Frick, D. N., Weber, D. J., Gillespie, J. R., Bessman, M. J., and Mildvan, A. S. (1994) *J. Biol. Chem.* 269(3), 1794-1803
69. Shimokawa, H., Fujii, Y., Furuichi, M., Sekiguchi, M., and Nakabeppu, Y. (2000) *Nucleic Acids Res.* 28(17), 3240-3249
70. Harris, T. K., Wu, G., Massiah, M. A., and Mildvan, A. S. (2000) *Biochemistry* 39(7), 1655-1674
71. Mildvan, A. S., Xia, Z., Azurmendi, H. F., Saraswat, V., Legler, P. M., Massiah, M. A., Gabelli, S. B., Bianchet, M. A., Kang, L. W., and Amzel, L. M. (2005) *Arch Biochem Biophys* 433(1), 129-143
72. Thompson, J. D., Higgins, D. G., and Gibson, T. J. (1994) *Nucleic Acids Res.* 22(22), 4673-4680

FOOTNOTES

* This work was supported in part by Grants-in-Aid for Scientific Research and the National Project for Protein Structural and Functional Analysis from the Ministry of Education, Culture, Sports, Sciences and Technology of Japan.

The abbreviations used are: 8-oxoG, 8-oxoguanine; Nudix, nucleoside diphosphate linked to some other moiety, X; SLHL, strand-loop-helix-loop; rmsd, root-mean-square deviations; ITC, isothermal titration calorimetry; ADPRase, adenosine 5′-diphosphoribose pyrophosphatase; Ap_4A hydrolase, diadenosine 5′, 5‴-P^1, P^4-tetraphosphate pyrophosphohydrolase; AMPCPP, adenosine 5′-(α, β-methylenetriphosphate).

The atomic coordinates and structure factors have been deposited in the Protein Data Bank, www.pdb.org (PDB ID 3A6S, 3A6T, 3A6U, and 3A6V).

Table 1. Data collection statistics.

Diffraction data	MutT				MutT–8-oxo-dGMP	MutT–8-oxo-dGMP–Mn^{2+}
	Native	Peak	Edge	Remote		
Beam line	SPring-8 BL41XU		PF BL18B		SPring-8 BL41XU	SPring-8 BL40B2
Wavelength (Å)	0.7080	0.9793	0.9791	0.9500	0.9000	1.296
Space group	$P2_1$		$P2_1$		$P2_12_12_1$	$P2_12_12_1$
Unit-cell lengths (Å, °)	a = 33.9 b = 71.6 c = 55.8 β = 99.0		a = 34.1 b = 71.1 c = 55.7 β = 98.7		a = 37.9 b = 56.0 c = 59.4	a = 38.2 b = 56.0 c = 59.3
Resolution range (Å)	20.0-1.8 (1.9-1.8)		20.0-2.2 (2.3-2.2)		20.0-1.96 (2.08-1.96)	18.56-2.56 (2.72-2.56)
No. of observed reflections	85,618	49,308	49,226	50,094	54,195	26,502
No. of unique reflections	24,217	13,041	13,015	13,147	9,344	4,395
Completeness (%)	99.7 (99.7)	97.2 (97.2)	97.3 (97.3)	98.3 (98.3)	97.6 (93.2)	99.2 (95.7)
[a] R_{merge} (%)	3.1 (9.4)	3.9 (12.1)	3.8 (12.3)	3.9 (12.1)	6.5 (18.1)	7.7 (15.2)
<I / sigmaI>	15.8 (7.9)	8.8 (3.3)	9.4 (5.0)	8.8 (5.6)	29.6 (6.2)	45.9 (22.6)

Values in parentheses correspond to the highest resolution shell.

[a] $R_{merge} = 100 \times \Sigma \mid I_{hkl} - \langle I_{hkl} \rangle \mid / \Sigma I_{hkl}$, $\langle I_{hkl} \rangle$ is the mean value of I_{hkl}.

Table 1. Data collection statistics. (*continued*)

Diffraction data	MutT-Mn^{2+}
Beam line	PF BL18B
Wavelength (Å)	1.000
Space group	$P2_1$
Unit-cell lengths (Å, °)	a = 35.8
	b = 56.0
	c = 74.1
	β =96.4
Resolution range (Å)	40.0-2.0 (2.03-2.00)
No. of observed reflections	77,213
No. of unique reflections	19,810
Completeness (%)	98.1 (96.2)
[a] R_{merge} (%)	4.2 (6.4)
<*I* / sigma*I*>	28.6 (18.6)

Values in parentheses correspond to the highest resolution shell.

[a] R_{merge} = 100 x Σ | I_{hkl} - <I_{hkl}> | / Σ I_{hkl}, <I_{hkl}> is the mean value of I_{hkl}.

Table 2. Refinement statistics.

Diffraction data	MutT	MutT–8-oxo-dGMP	MutT–8-oxo-dGMP –Mn^{2+}	MutT-Mn^{2+}
Resolution range (Å)	20.0-1.8	20.0-1.96	18.56-2.56	20.0-2.0
Number of reflections used	24,213	9,280	4,394	19,386
Number of atoms				
Protein	2,025	1,038	1,029	2,010
Water	190	136	92	131
Nucleotide	0	24	24	0
Mn^{2+} ion	0	0	1	4 [b]
Other	11	34	5	32
Completeness (%)	99.1	97.3	99.9	98.1
R_{cryst} /R_{free} [a] (%)	20.4/23.1	17.8/20.1	19.3/24.2	19.2/22.7
Ramachandran plot (%)				
Most favored	93.0	91.5	87.6	94.9
Additional allowed	7.0	8.5	12.4	5.1
Generously allowed	0	0	0	0
Disallowed	0	0	0	0
R.m.s.d. in bonds (Å)	0.005	0.005	0.007	0.005
R.m.s.d. in angles (deg.)	1.2	1.3	1.3	1.2

[a] $R_{cryst} = 100 \times \Sigma \, | \, | F_o | - | F_c | \, | \, / \, \Sigma \, | F_o |$. R_{free} was calculated from the test set (5% of the total data).

[b] 2 ions per monomer.

FIGURE LEGENDS

Fig. 1. Sequence alignment of MutT family proteins. Amino acid sequences of MutT family proteins were aligned using Clustal W (72). MutT homologs from species related to *E. coli*, which share high sequence similarity, were chosen and are listed. They are from *E. coli* (CAA28523), *Yersinia pestis* (NP_670913), *Proteus mirabilis* (ZP_03840798), *Providencia rustigianii* (ZP_03315124), *Vibrio cholerae* (NP_232022), and *Pseudomonas aeruginosa* (ZP_04932260). In addition to *E. coli* MutT, *E. coli* Orf135 (BAA15549), human MTH1 (BAA07601), and *B. subtilis* YtkD (NP_390941), which have 8-oxo-dGTPase activity *in vitro,* were added and are shown in red. Absolutely conserved residues are shown in red, and identical residues are in pink. The green asterisks on the *E. coli* MutT sequence indicate amino residues that participate in the recognition of 8-oxoG and the ligand-induced conformational change. The secondary structure of *E. coli* MutT in the apo form is shown at the top. The α-helices, β-strands, and 3_{10} helices are represented as red bars, blue arrows, and pink bars, respectively.

Fig. 2. Crystal structures of MutT apo and MutT-8-oxo-dGMP complex forms. (A) Overall structure of MutT. α-helices are in pink, and β-strands in slate. A missing region of L-A is shown as a gray dashed line. (B) Overall structure of MutT-8-oxo-dGMP. 8-Oxo-dGMP is shown in ball and stick representation. (C) Comparison of the structures of the apo and complex forms. Apo and complex forms are shown in gray and slate, respectively. L-A and L-D regions in MutT-8-oxo-dGMP adopt a closed conformation as compared to those in the apo form.

Fig. 3. Recognition of 8-oxo-dGMP by MutT. (A) Hydrogen bonding interactions between 8-oxo-dGMP and loop regions (apo in gray and MutT-8-oxo-dGMP in slate). Amino acid residues involved in the hydrogen bonding interactions are shown in ball and stick representation. Water molecules are in red. Hydrogen bonds are shown as yellow dashed lines. (B) The hydrophobic cave composed of β-1, β-3, β-3′, β-5, and α-2 is represented as a translucent surface (carbon in white, nitrogen in cyan, and oxygen in pink). (C) Interactions for the *syn* conformation of 8-oxo-dGMP. The hydrogen bond between Oδ of Asn119 and N7-H of 8-oxoG is shown as a red dashed line. (D) Van der Waals interactions around the O8 atom. Amino acid residues recognizing O8 are shown in ball, stick, and translucent surface. (E) A $2F_o - F_c$ electron density map around 8-oxo-dGMP contoured at 1.5σ (stereo view).

Fig. 4. Coordination scheme of Mn^{2+} at the MutT signature in MutT-8-oxo-dGMP-Mn^{2+} and MutT-Mn^{2+}. (A) The coordination scheme of Mn^{2+} and the structure of the MutT signature in MutT-8-oxo-dGMP-Mn^{2+}. Mn^{2+} in blue has an ideal octahedral coordination with Gly37, Glu57, Pα-O of 8-oxo-dGMP, and water molecules. The hydrogen bonding interactions shown in yellow dashed lines contribute to the conformational stabilization of the SLHL structure of the MutT signature. The SLHL structure is in pink. (B) The coordination scheme of Mn^{2+} in MutT-Mn^{2+}. Na^{+} is shown in green. Asp77* is an amino acid of another molecule in the asymmetric unit. (C) Superposition of two Mn^{2+} ions in MutT-Mn^{2+} onto the structure of MutT-8-oxo-dGMP-Mn^{2+} (stereo view). Coloring is as in Fig. 4A. Mn^{2+} ions observed in MutT-Mn^{2+} are shown in cyan (Mn2 and Mn3).

Fig. 1

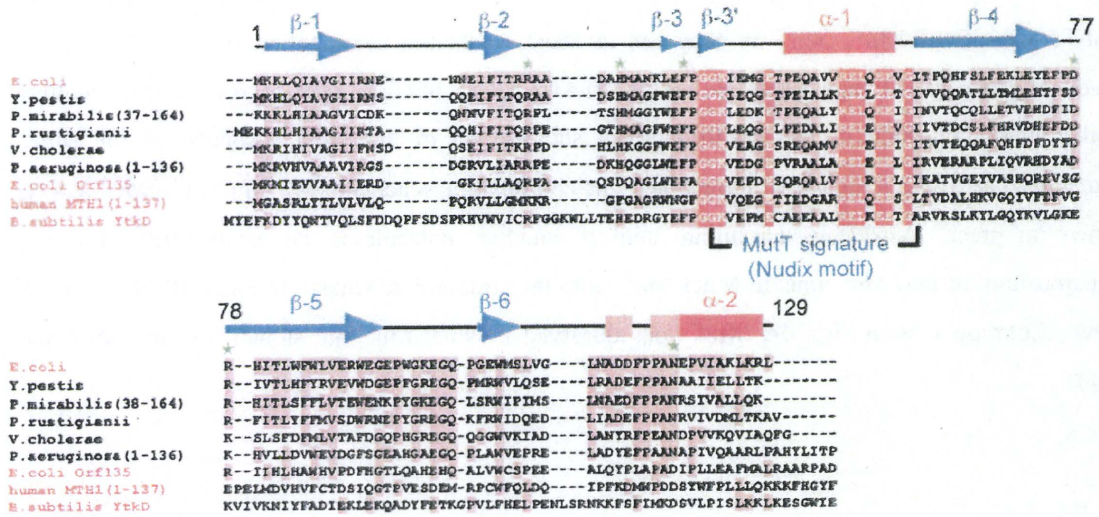

Fig. 2

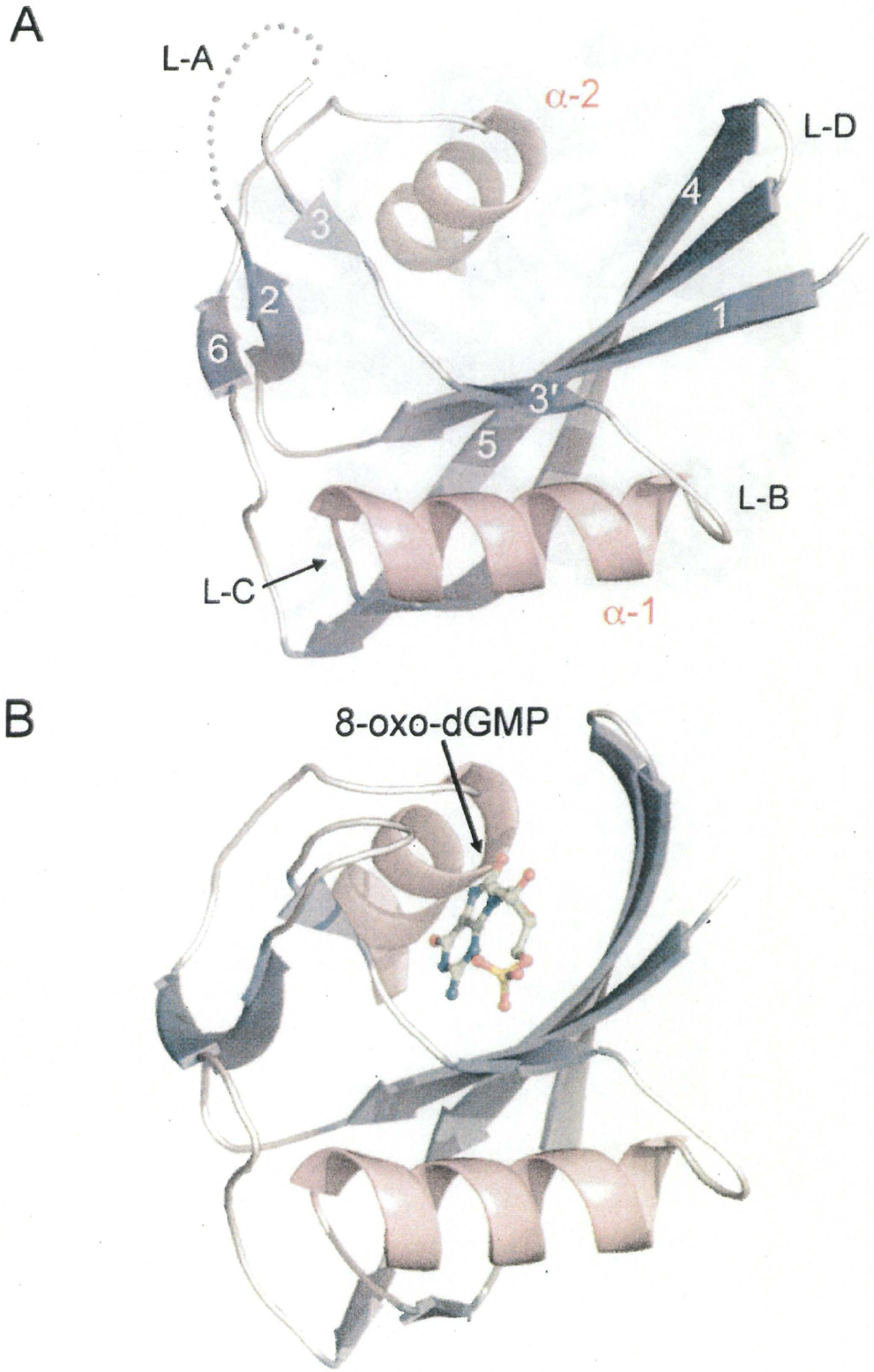

Fig. 2

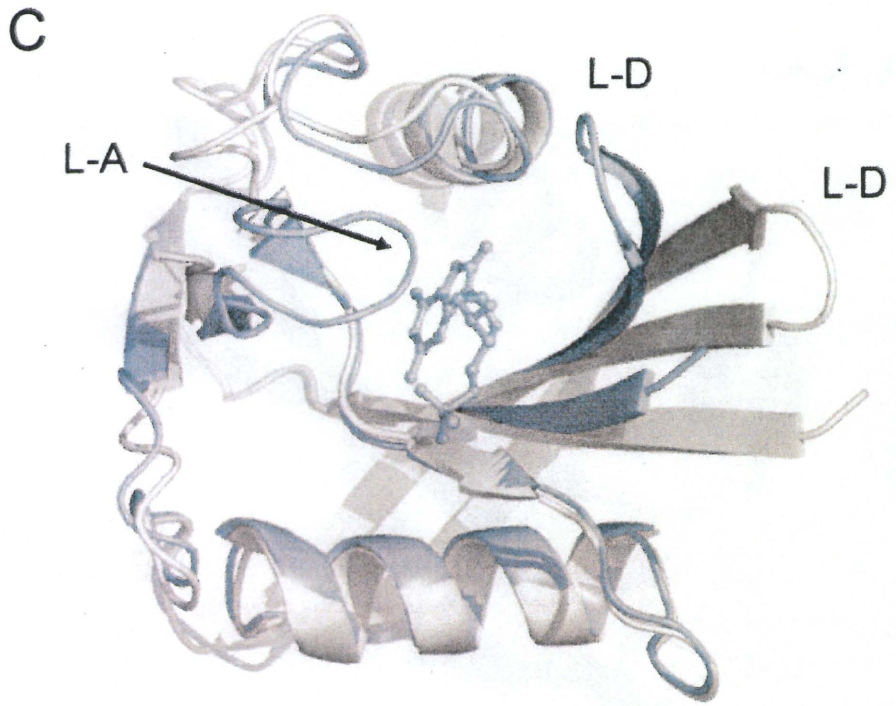

Fig. 3

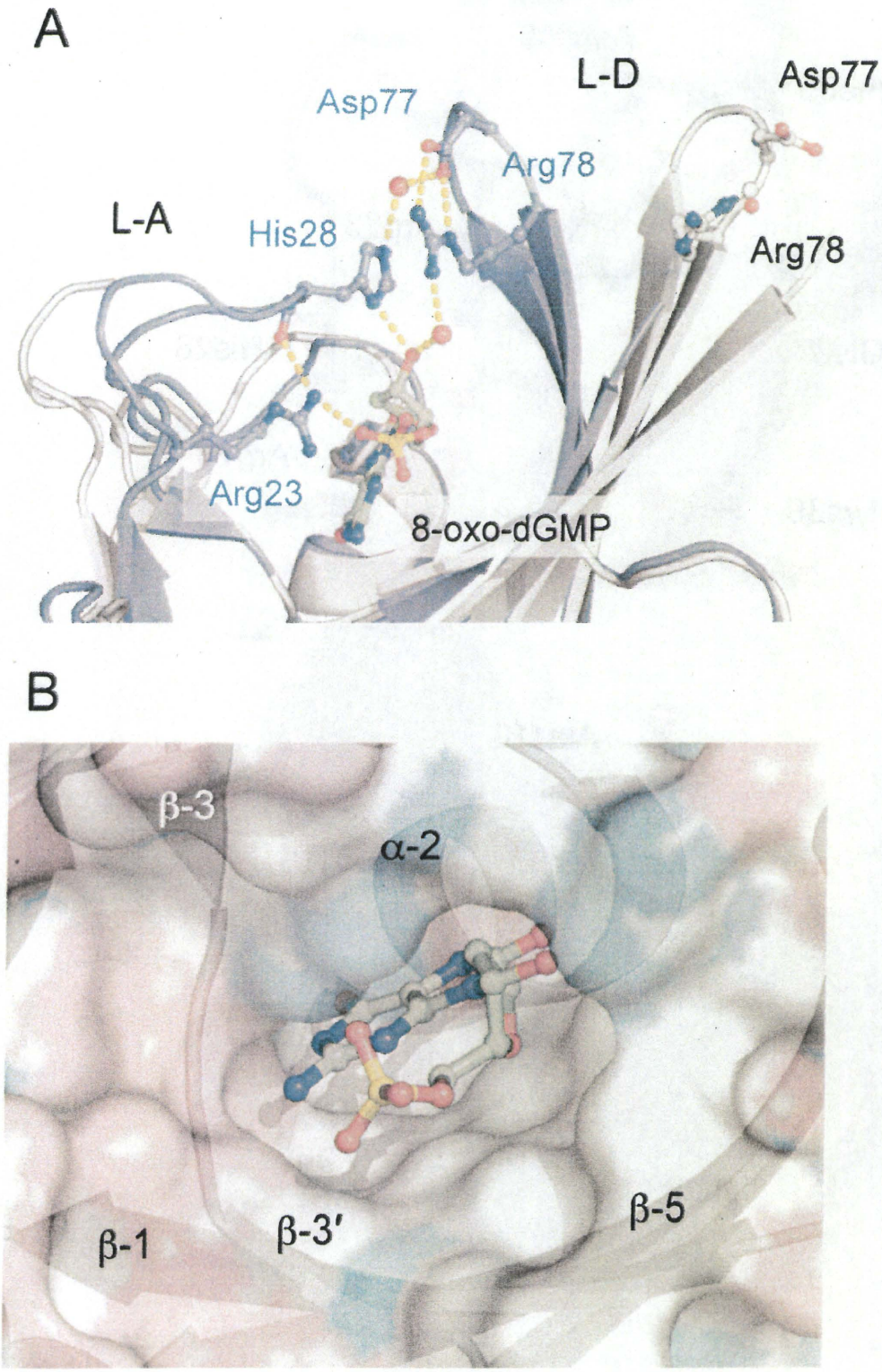

Fig. 3

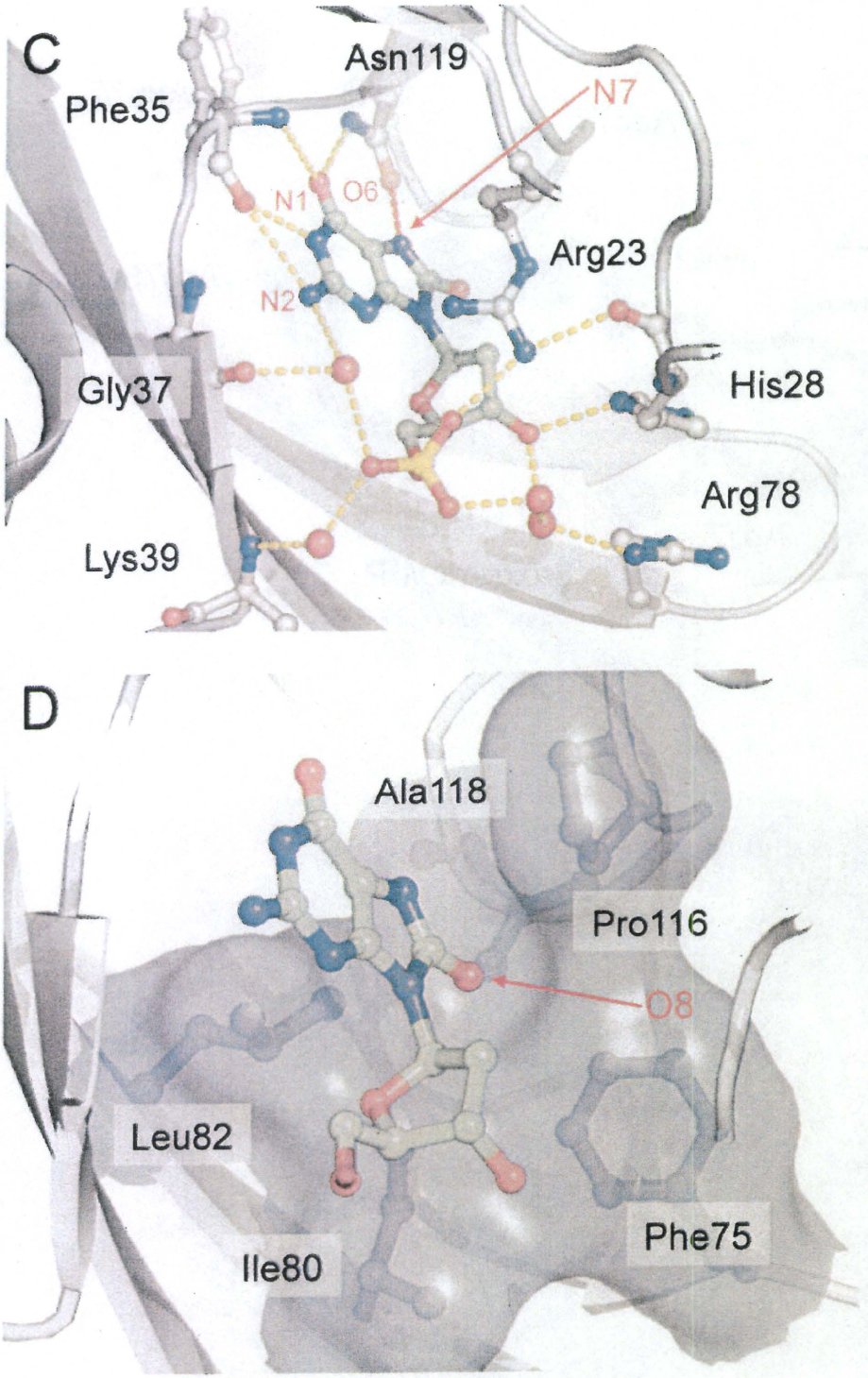

Fig. 3

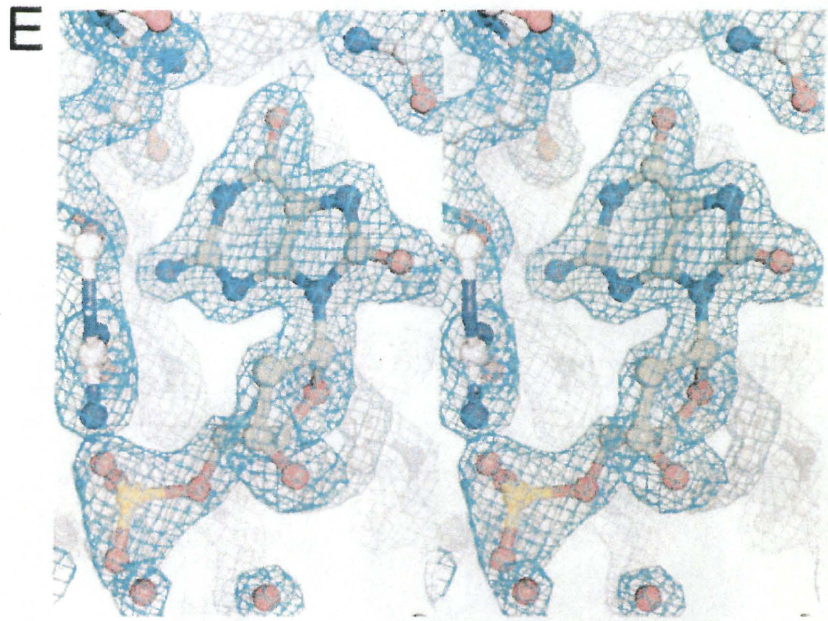

Fig. 4